Medical Engineering & Physics xxx (2012) xxx–xxx

Contents lists available at SciVerse ScienceDirect

Medical Engineering & Physics

journal homepage: www.elsevier.com/locate/medengphy

Simulation model of cardiac three dimensional accelerometer measurements

Espen W. Remme[a,c,*], Lars Hoff[b], Per Steinar Halvorsen[a], Anders Opdahl[c], Erik Fosse[a,e], Ole Jakob Elle[a,d]

[a] The Intervention Center, Oslo University Hospital, Rikshospitalet, Oslo, Norway
[b] Vestfold University College, Tønsberg, Norway
[c] Institute for Surgical Research, Oslo University Hospital, Rikshospitalet, Oslo, Norway
[d] Department of Informatics, University of Oslo, Oslo, Norway
[e] Institute for Clinical Medicine, Faculty of Medicine, University of Oslo, Oslo, Norway

ARTICLE INFO

Article history:
Received 11 August 2011
Received in revised form 18 April 2012
Accepted 28 April 2012

Keywords:
Biomedical sensor
Accelerometer
Cardiac surgery
Cardiac simulation model

ABSTRACT

A miniaturized accelerometer sensor attached to the heart may be applied for monitoring cardiac motion. Proper understanding of the sensor measurements is required for successful development of algorithms to process the signal and extract clinical information. In vivo testing of such sensors is limited by the invasive nature of the procedure. In this study we have developed a mathematical simulation model of an accelerometer attached to the heart so that testing initially may be performed on realistic, simulated measurements. Previously recorded cardiac motion by sonomicrometric crystals was used as input to the model. The three dimensional motion of a crystal attached to the heart served as the simulated motion of the accelerometer, providing the translational acceleration components. A component of gravity is also measured by the accelerometer and fused with the translational acceleration. The component of gravity along an accelerometer axis varies when the axis direction slightly rotates as the accelerometer moves during the cardiac cycle. This time-varying gravity component has substantial effects on the accelerometer measurements and was included in the simulation model by converting the motion to prolate spheroidal coordinates where the axis rotation could be found. The simulated accelerometer signal was filtered and integrated to velocity and displacement. The resulting simulated motion was consistent with previous accelerometer recordings during normal and ischemic conditions as well as for alterations of accelerometer orientation and patient positions. This suggests that the model could potentially be useful in future testing of algorithms to filter and process accelerometer measurements.

1. Introduction

Previous studies have indicated that an accelerometer sensor attached to the heart wall may be used to measure cardiac motion and automatically detect motion abnormalities that occur during myocardial dysfunction [1–3]. Thus, an accelerometer sensor may be useful for continuously monitoring patients who undergo cardiac surgery as the accelerometer could immediately detect myocardial dysfunction occurring during surgery or during the first few days following the operation [4]. Early detection of myocardial dysfunction has been shown to reduce complications and improve the prognosis for patients undergoing cardiac surgery [5]. Current methods to evaluate cardiac motion and detect ischemia during surgery are limited. Transesophageal echocardiography may be used but requires a skilled operator and only intermittent measurements are available. For the same reasons echocardiography or other imaging modalities are not routinely used in the postoperative phase. Hence, there is a need for new methods for continuous real-time monitoring of myocardial ischemia, and a solution may be a miniaturized accelerometer attached to the heart.

The ability of an accelerometer to detect motion abnormalities is likely dependent on its accuracy to measure true motion and its ability to do so in various settings such as different placements of the sensor and orientations of the patient, e.g. sitting, supine, or standing. Testing of the accelerometer performance in these different settings is important as the accelerometer measurements are influenced by gravity. The accelerometer cannot distinguish between a translational acceleration and a gravitational field as acceleration and gravitation are equivalent. The accelerometer measures the vector sum of the translational acceleration and the gravitation. Hence, for each of the three accelerometer axes, the projection of the gravitation vector along this axis is added to the translational acceleration. If the accelerometer rotates, its orientation relative to the gravity field is changed, resulting in a change in accelerometer output. A static component of gravity may be removed from the measurement by high-pass filtering. However, in a previous study we found that the gravity component along an axis of the accelerometer is generally not static [6]. An axis of the

* Corresponding author at: The Intervention Center, Oslo University Hospital, Rikshospitalet, Postbox 4950 Nydalen, 0424 Oslo, Norway. Tel.: +47 2307 1413; fax: +47 2307 1397.
E-mail address: espen.remme@medisin.uio.no (E.W. Remme).

1350-4533/$ – see front matter © 2012 IPEM. Published by Elsevier Ltd. All rights reserved.
http://dx.doi.org/10.1016/j.medengphy.2012.04.015

accelerometer typically changes its orientation relative to the vertical direction during the cardiac cycle, introducing a time-varying gravity artifact that has substantial effect on the accuracy of the accelerometer. This change in orientation is typically periodic, with the heart rate as fundamental frequency; hence, it cannot be removed from the translational acceleration by linear filtering. In our previous validation study [6] we found that when the gravitational component was correctly accounted for, cardiac velocity and displacement could be calculated from the measured accelerometer signal with very high accuracy (typically an error < 1%).

Generally, the direction of gravity relative to the orientation of the accelerometer will vary with the different settings, and thus alter the measured signal. In vivo testing of the accelerometer in animals and humans is expensive and time-consuming. Few situations may be tested in each subject due to the invasive nature of the procedure. By first performing theoretical analyses using mathematical simulation models of the heart and accelerometer sensor, the number of in vivo tests may be reduced and optimized. Development of such simulation models requires information of both cardiac motion and understanding of what the sensor actually measures.

The aim of this study was to develop a realistic 3 dimensional (3D) kinematic simulation model of cardiac motion for testing of accelerometer performance and potential new algorithms to filter and process the accelerometer signal in a controlled environment where the ground truth motion is known. We applied the model to test how gravity affected the accuracy of the accelerometer measurements during different situations and investigated if the results were consistent with a previous validation study of the accelerometer. In the previous validation study [6] we attached the accelerometer to a robot arm programmed to move like a point on the heart wall during different situations, and we also compared measured velocity and displacement from the accelerometer attached to pig hearts with other reference methods. In the current study, we finally compared if the changes seen in the simulated signal from baseline to ischemia were consistent with previously recorded measurements in pigs where ischemia was acutely introduced [13].

2. Methods

2.1. Background on cardiac motion and accelerometer measurements

Technical specifications of the accelerometer and signal processing of the measured signal are described in previous publications [7,8]. The accelerometer sensor is designed so that it may be attached to the outer surface of the heart. The surface of the ventricles may be approximated as a circular, truncated ellipse. Due to the elliptical shape, the geometry of the heart is described in elliptical notation: circumferential, longitudinal and radial directions. The ventricular walls undergo large deformations during the cardiac cycle. During ejection the ventricular wall shortens in the circumferential and longitudinal directions, while there is thickening of the wall in the radial direction; all deformations contributing to the reduction of the cavity volumes. In the subepicardium the myofibers run at an oblique angle with respect to the circumferential direction. Contraction of these fibers twists the ventricular wall, rotating the base clockwise and the apical region counterclockwise as viewed from an apical perspective. Over the cardiac cycle the measured rotation trace of an apical short-axis plane looks approximately like a half sinusoidal wave peaking at $13 \pm 4^{\circ}$ in the healthy human heart, while it may be significantly reduced and with regional variations in the ischemic case [9]. Due to the curved surface and the rotations, an accelerometer placed on the surface will generally change the orientation of its axes with respect to gravity as it is moved with the wall during the cardiac cycle. The measured acceleration (a_i) along an axis i ($i \in 1,2,3$) of the accelerometer is:

$$a_i(t) = \mathbf{a}(t) \cdot \mathbf{e_i}(t) - \mathbf{g} \cdot \mathbf{e_i}(t) \quad (1)$$

where $\mathbf{a}$ is the 3D acceleration of the point where the accelerometer is attached, $\mathbf{e_i}$ is the direction vector of the accelerometer axis i and $\mathbf{g}$ is the vertical gravity vector. Note that a stationary accelerometer with an axis pointing upwards (opposite of $\mathbf{g}$) will measure +1g while it would measure 0g if the accelerometer was falling freely. Eq. (1) does not include a term that accounts for motion of the patient, so the system is limited to a situation where the patient is in a stationary position.

The velocity and displacement of the accelerometer during one heartbeat can be found by integration of the accelerometer signal. Over one heartbeat it may be assumed that every point on the heart starts and returns to the same position in space which is equivalent to zero mean acceleration and velocity. Hence, prior to integration to velocity, the mean acceleration over one heartbeat may be subtracted from the acceleration signal, which takes care of the integration constant and avoids the potential problem of long-term drifting of the accelerometer signal. Similarly, mean velocity may be subtracted from the resulting velocity signal prior to integration to displacement. This procedure also eliminates a static component of gravity, and provides the true velocity and displacement if the accelerometer orientation is fixed relative to the direction of gravity. However, as demonstrated in our previous study [6], the gravity component, the second term in Eq. (1), is not static. Subtraction of the mean acceleration over one cardiac cycle does not totally remove the gravity term of Eq. (1), but effectively replaces the last term with the remaining time-varying gravity component. This time-varying gravity term is added together with the first term (the true translational acceleration) and hence introduces errors when the resulting acceleration (sum of the 2 terms) is integrated to velocity and displacement. The impact of this error may affect the performance of the sensor, including its ability to automatically detect motion abnormalities.

2.2. Database of measured cardiac motion

Measurements of cardiac motion from previous studies of 7 dogs [10] were used in the development of the simulation model. The surgical preparation of these animals has been described previously [11]. In short, in an open chest model sonomicrometric crystals (Sononmetrics, London, Ontario, Canada) were implanted in the myocardium at specified locations as shown in Fig. 1. Each crystal can both send and receive sound. The sound travels at approximately 1560 m/s in both blood and myocardium. The distance between 2 crystals is calculated from the measured time-of-flight for a sound pulse transmitted from one crystal until it is received by the other. The different distances between the crystals were sampled at 200 Hz.

During post-processing of the data, the crystal software (CardioSoft, Sononmetrics, London, Ontario, Canada) allowed calculation of the time-varying positions in space of each crystal. To perform this calculation one crystal had to be chosen as the stationary origin, while two other crystals were chosen to specify the x-axis and xy-plane of the crystals, respectively. A third crystal was selected to specify the orientation of the z-axis. With these input conditions the software calculated the time-varying positions of the crystals from the transmit time measurements, using a least-squares procedure to fit the different measurements. The result was the time-varying positions of the crystals relative to one another in the specified coordinate system where the selected crystal representing the origin was stationary through the cardiac cycle. However, all crystals in the myocardium are generally moving in the real heart. Hence, we used custom made

Please cite this article in press as: Remme EW, et al. Simulation model of cardiac three dimensional accelerometer measurements. Med Eng Phys (2012), http://dx.doi.org/10.1016/j.medengphy.2012.04.015

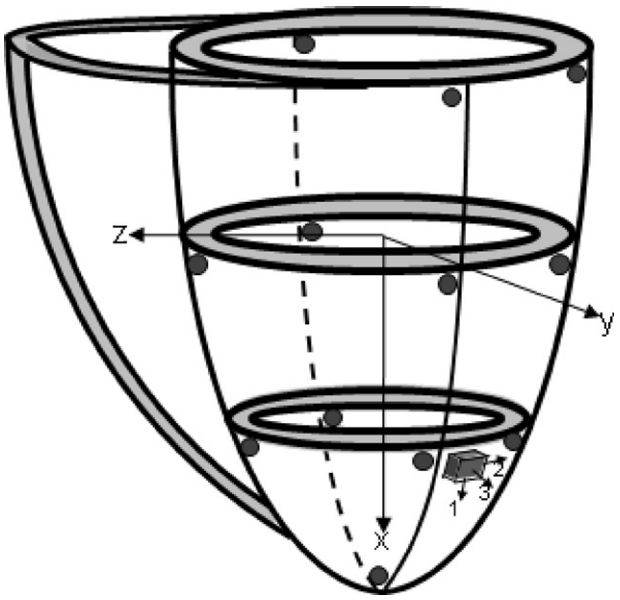

Fig. 1. Schematic illustration of the crystal placement (spheres) around the left ventricle. The illustration also shows the standard positioning and orientation of an accelerometer (box) in the apical, anterior region with axis 1 in the longitudinal direction, axis 2 in the circumferential direction and axis 3 in the radial direction.

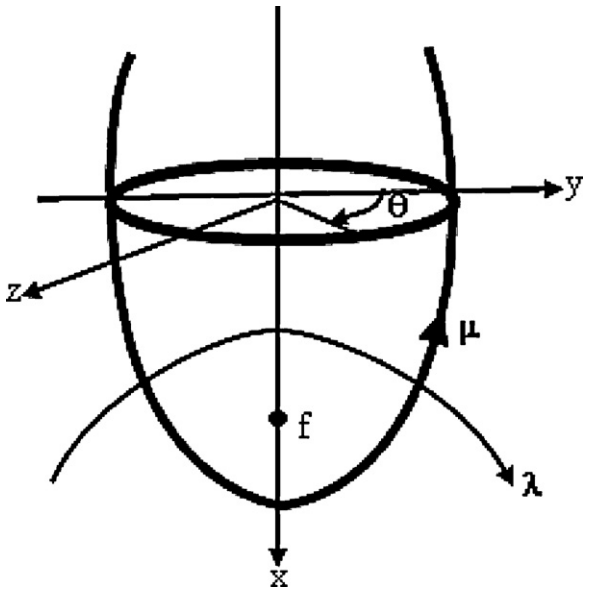

Fig. 2. Prolate spheroidal coordinates. The direction of the circumferential (θ), longitudinal (μ) and radial (λ) coordinates is shown together with the focus (f) which scales the size of the geometry.

software [11] to calculate another point in the middle of the equatorial plane of the left ventricle (approximately the center of mass of the ventricle). This point was selected as the stationary origin and the coordinates of the crystals were transformed to this coordinate system. As a result the time-varying x,y,z-coordinates of each crystal relative to this stationary origin was found where the x-axis pointed in the direction of the apex and the crystal in the anterior wall in the most apical crystal plane was lying on the positive y-axis at the start of the cycle (R-peak of the ECG) (Fig. 1).

2.3. Development of a mathematical model of cardiac motion and simulated accelerometer measurements

The 3D motion of a crystal, i.e. the $x(t)$, $y(t)$, $z(t)$-coordinates of the crystal, was used to represent the motion of an accelerometer attached to that point on the heart. In principle, motion of any of the crystals at the different locations could be used. In our previous studies with accelerometer in pigs and humans, the accelerometer was placed in the apical, anterior region (LAD perfusion territory), which is easily accessible for the surgeon and a region that we believe will be most affected by abnormal motion. Therefore, we selected the crystal placed in this region (Fig. 1) to represent the accelerometer motion. The simulated translational acceleration was calculated by twice differentiation of the time-varying position of the crystal. This differentiation provided the 3D acceleration, i.e. $\mathbf{a}(t)$ in the first term of Eq. (1).

The accelerometer axes are generally not aligned with the x,y,z-axes and their orientation vary as the accelerometer moves with the heart during the cardiac cycle. To calculate the simulated acceleration signal along each axes of the accelerometer, $a_i(t)$, the time-varying orientations ($\mathbf{e_i}$) of the accelerometer axes were found by applying a prolate spheroidal (PS) coordinate system. The approximately truncated circular ellipsoidal geometry of the heart may be represented by PS coordinates as shown in Eq. (2) and Fig. 2 [12].

$$\begin{aligned} x &= f \cdot \cosh(\lambda)\cos(\mu) \\ y &= f \cdot \sinh(\lambda)\sin(\mu)\cos(\theta) \\ z &= f \cdot \sinh(\lambda)\sin(\mu)\sin(\theta) \end{aligned} \tag{2}$$

The PS coordinate axes are aligned in the circumferential (θ), longitudinal (μ), and radial (λ) directions of the heart. We scaled the focal length of the coordinate system, f, to the crystal data of each individual heart. This was performed by first measuring left ventricular radius at the equatorial plane (found from a circle fitted to the position of 4 crystals around the equator). We arbitrarily chose that λ should be equal to 0.75 for this circle and the focal length was found as f = radius/sin$h$(0.75), corresponding to a point on equator where $\mu = 90^\circ$ and $\theta = 0^\circ$. The orthogonal direction vectors of the θ, μ and λ coordinate axes on the prolate spheroidal surface change orientation as a function of position on the surface. These PS coordinate base vectors in rectangular Cartesian (RC) coordinates ($\mathbf{u_p}$, $p \in (\theta, \mu, \lambda)$) and their unit direction vectors ($\mathbf{e_p}$) are found as the derivative of x, y and z with respect to θ, μ and λ as shown in Eq. (3). The derivatives are found by differentiations of Eq. (2).

$$\begin{aligned} \mathbf{u}_\theta &= \left[\frac{\partial x}{\partial \theta}, \frac{\partial y}{\partial \theta}, \frac{\partial z}{\partial \theta}\right], \quad \mathbf{e}_{\boldsymbol{\theta}} = \frac{\mathbf{u}_{\boldsymbol{\theta}}}{|\mathbf{u}_{\boldsymbol{\theta}}|} \\ \mathbf{u}_\mu &= \left[\frac{\partial x}{\partial \mu}, \frac{\partial y}{\partial \mu}, \frac{\partial z}{\partial \mu}\right], \quad \mathbf{e}_{\boldsymbol{\mu}} = \frac{\mathbf{u}_{\boldsymbol{\mu}}}{|\mathbf{u}_{\boldsymbol{\mu}}|} \\ \mathbf{u}_\lambda &= \left[\frac{\partial x}{\partial \lambda}, \frac{\partial y}{\partial \lambda}, \frac{\partial z}{\partial \lambda}\right], \quad \mathbf{e}_{\boldsymbol{\lambda}} = \frac{\mathbf{u}_{\boldsymbol{\lambda}}}{|\mathbf{u}_{\boldsymbol{\lambda}}|} \end{aligned} \tag{3}$$

The 3 orthonormal direction vectors ($\mathbf{e_\theta}$, $\mathbf{e_\mu}$, $\mathbf{e_\lambda}$) are aligned with the circumferential, longitudinal and radial directions, respectively, at any point of the prolate spheroidal surface. Thus, by converting the time-varying x,y,z-coordinates of the accelerometer to θ,μ,λ-coordinates for every time-step, the change of the accelerometer axis vectors would be approximately parallel to the change in the direction vectors $\mathbf{e_\theta}$, $\mathbf{e_\mu}$, $\mathbf{e_\lambda}$ for every time-increment. We utilized this property to simulate the time varying orientation of the accelerometer direction vectors: at every x,y,z position of the accelerometer the corresponding $\mathbf{e_\theta}$, $\mathbf{e_\mu}$, $\mathbf{e_\lambda}$ were found and $\mathbf{e_1}$, $\mathbf{e_2}$, $\mathbf{e_3}$ were subsequently calculated by maintaining a fixed angle of these vectors in relation to the PS base vectors. The orientation of the orthogonal accelerometer axes was specified with respect to the θ, μ, λ directions as desired. This allowed simulation of the accelerometer signal for different cases of how the accelerometer was oriented when it was attached to the heart by the surgeon, e.g.

Please cite this article in press as: Remme EW, et al. Simulation model of cardiac three dimensional accelerometer measurements. Med Eng Phys (2012), http://dx.doi.org/10.1016/j.medengphy.2012.04.015

mimicking attachment with accelerometer axis #2 parallel with the circumferential direction of the heart (as in Fig. 1) or for example 15° off. This further allowed investigation of how accelerometer orientation affected the accuracy of the derived velocity and displacement measurements.

The procedure to generate simulated accelerometer signals can be summarized as:

1. Extract the time-varying x,y,z position of a crystal which represents the attached accelerometer
2. Calculate the acceleration of this point, $\mathbf{a}(t)$
3. Convert the RC coordinates to PS coordinates and find the PS base vectors, $(\mathbf{e}_\theta, \mathbf{e}_\mu, \mathbf{e}_\lambda)$
4. Calculate the orientation of the accelerometer direction vectors $(\mathbf{e_1}, \mathbf{e_2}, \mathbf{e_3})$ from their prescribed, fixed orientation relative to the PS base vectors
5. Calculate the translational acceleration term, $\mathbf{a}(t)\cdot\mathbf{e_i}(t)$
6. Calculate the gravity component, $\mathbf{g}\cdot\mathbf{e_i}(t)$, where the orientation of gravity has been prescribed according to the desired orientation of the heart (i.e. patient in a supine, sitting or standing position)
7. The difference of the 2 terms from points 5 and 6 serves as the simulated accelerometer signal as shown in Eq. (1)

2.4. Filter for removal of the time-varying gravity component

We have previously proposed a filter for removal of the artifact caused by the time-varying gravity component along the circumferential direction as described in detail in [6]. Briefly, the filter is based on the assumption that an accelerometer in the apical region moves along a purely circular path with radius R and time-varying rotation angle (α). The long-axis of the heart is presumed to have a stationary angle, β, with respect to the horizontal direction. We derived an algorithm to estimate α and β, i.e. α_{est} and β_{est}, respectively. This allowed estimation of the time-varying gravity component which was subtracted from the measured acceleration signal in order to extract the pure translational acceleration, $a_{2t}(t)$, in the circumferential direction as shown in Eq. (4). In the former study we did not validate radial or longitudinal displacement. However, the centripetal and gravity components can be removed from the radial acceleration signal as shown in Eq. (5) to estimate the pure translational radial acceleration component. The filtered displacements can be found by double integration of the acceleration signal. Circumferential displacement can also be calculated directly as the fraction of the circumference traveled by the rotation along the circle as shown in Eq. (6). The algorithm requires measurement of radius, R, which in the simulation model can be calculated as the radius of the best-fitted circle to the 4 crystals in the apical plane at end diastole. The proposed filtering algorithm to remove the time-varying gravity artifact only works in the circumferential and radial directions, thus longitudinal acceleration is not filtered.

$$a_{2t}(t) \approx a_2(t) + g\ \cos(\alpha_{est}(t))\cos(\beta_{est}) \quad (4)$$

$$a_{3t}(t) \approx a_3(t) + R\dot{\alpha}_{est}(t)^2 - g\ \sin(\alpha_{est}(t))\cos(\beta_{est}) \quad (5)$$

$$d_2(t) \approx -2R\pi\frac{(\alpha_{est}(t) - \alpha_{est}(0))}{2\pi} \quad (6)$$

2.5. Comparison of simulated measurements with previous results

We calculated the simulated measurements from an accelerometer placed in the LV anterior, apical region using data from 7 dogs as input to the algorithm described in Section 2.3. We investigated if the frequency components of the simulated acceleration signal were comparable to the frequency components from measured acceleration in real hearts. This investigation was performed by calculating the power spectrum of the simulated acceleration signal from each of the 7 animals and comparing these with the power spectra from actual accelerometer measurements in 12 pigs recorded in a previous study [13].

The simulated acceleration was integrated to velocity and displacement. We evaluated if the simulated velocity and displacement traces included the characteristic phases corresponding to systolic ejection, and early and late diastolic filling, e.g. the s′, e′ and a′ waves, respectively, which are typical observed in measured velocity traces.

We investigated if the simulation model provided similar results to the previous validation study with and without the filtering algorithm to remove the time-varying gravity component. This was first tested in the standard per-operative situation: the patient in a supine position with the accelerometer placed in the anterior, apical region with the accelerometer axis #2 parallel to the circumferential direction. We subsequently simulated other patient situations: patient sitting in a reclined position, standing patient, and patient lying on the left side. These situations were simulated by altering the relative orientation of the heart and direction of gravity: in the per-operative situation the gravity pointed in the negative y-axis direction in Fig. 1; in the reclined sitting position gravity pointed at 45° in the xy-plane with a positive x and negative y-component; in the standing position gravity pointed parallel to the x-axis; in the left lateral lying position gravity pointed in negative z-direction. Finally, we tested a situation where the accelerometer was incorrectly fastened to the epicardium, i.e. a misalignment of the accelerometer and the cardiac axes so the accelerometer axis #2 was 15° off from the circumferential direction. The simulated displacements were extracted using the measured crystal motion from each of the 7 animals as input to the simulation model, i.e. each situation with a different patient position or accelerometer placement was simulated 7 times. The measured crystal displacement was used as reference and compared with the simulated displacement of the accelerometer.

We extracted simulated measurements from the animals during baseline conditions and after 15 min of LAD occlusion. We compared the changes in the simulated measurements from baseline to ischemia with our previous study in pigs [13] where circumferential displacement and velocity were measured by accelerometer during baseline and ischemia.

3. Results

The power of the frequency components of the simulated acceleration signal was overall comparable to that from the measured acceleration signal. The power spectrum of the simulated signal laid for the most part within the same range as the spectrum of the measured acceleration as shown in Fig. 3.

The velocity and displacement traces derived from the simulated acceleration signal contained the characteristic systolic and diastolic waves that are typically seen in measurements. However, the wave corresponding to atrial induced filling of the ventricles was relatively low in most of the animals. This was probably due to the relatively high heart rate of the animals during the recordings (100 ± 20 beats/min) which caused most of the filling to occur during early filling or a fusion of early and late ventricular filling. Fig. 4 shows an example of the acceleration, velocity and displacement traces along each of the 3 axes of the accelerometer which in this simulation case were aligned in the standard orientation along the longitudinal, circumferential and radial directions. The online Supplement shows a movie with the simulated motion of the accelerometer sensor and visualizes the time-varying rotation of the accelerometer axes.

Please cite this article in press as: Remme EW, et al. Simulation model of cardiac three dimensional accelerometer measurements. Med Eng Phys (2012), http://dx.doi.org/10.1016/j.medengphy.2012.04.015

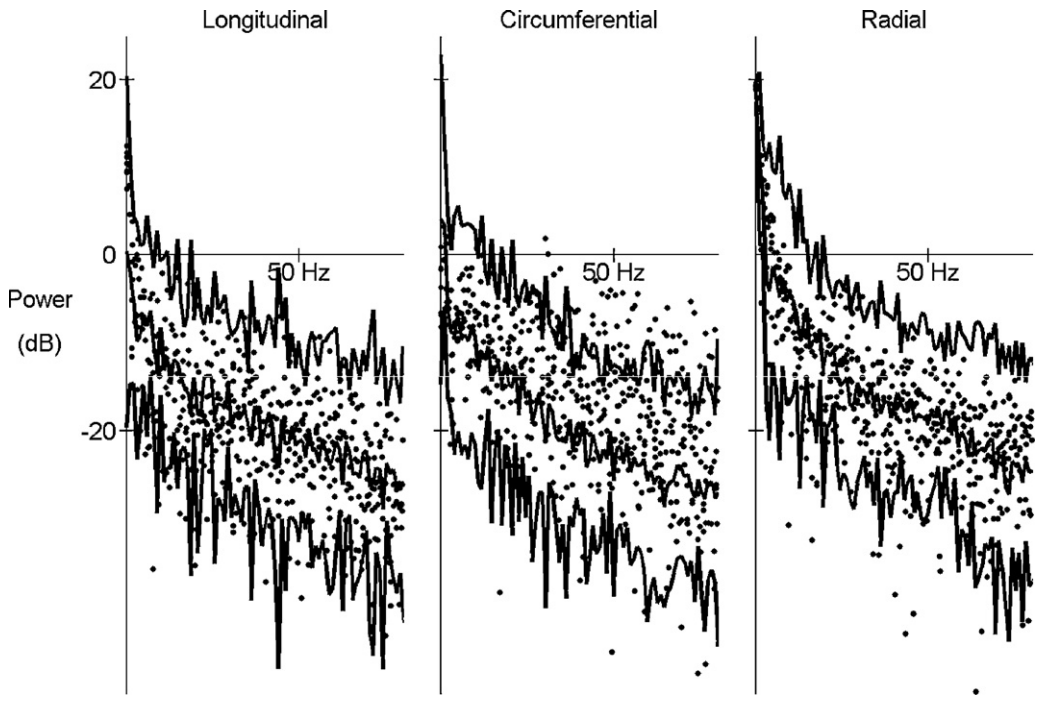

Fig. 3. Power spectrum of the signal from an accelerometer attached in the anterior apical region. The solid lines are the mean ± 2SD spectrum of measured accelerations in 12 pigs. The dots are the spectrum of the simulated acceleration signal using sonomicrometry recordings from 7 dogs as input to the simulation model.

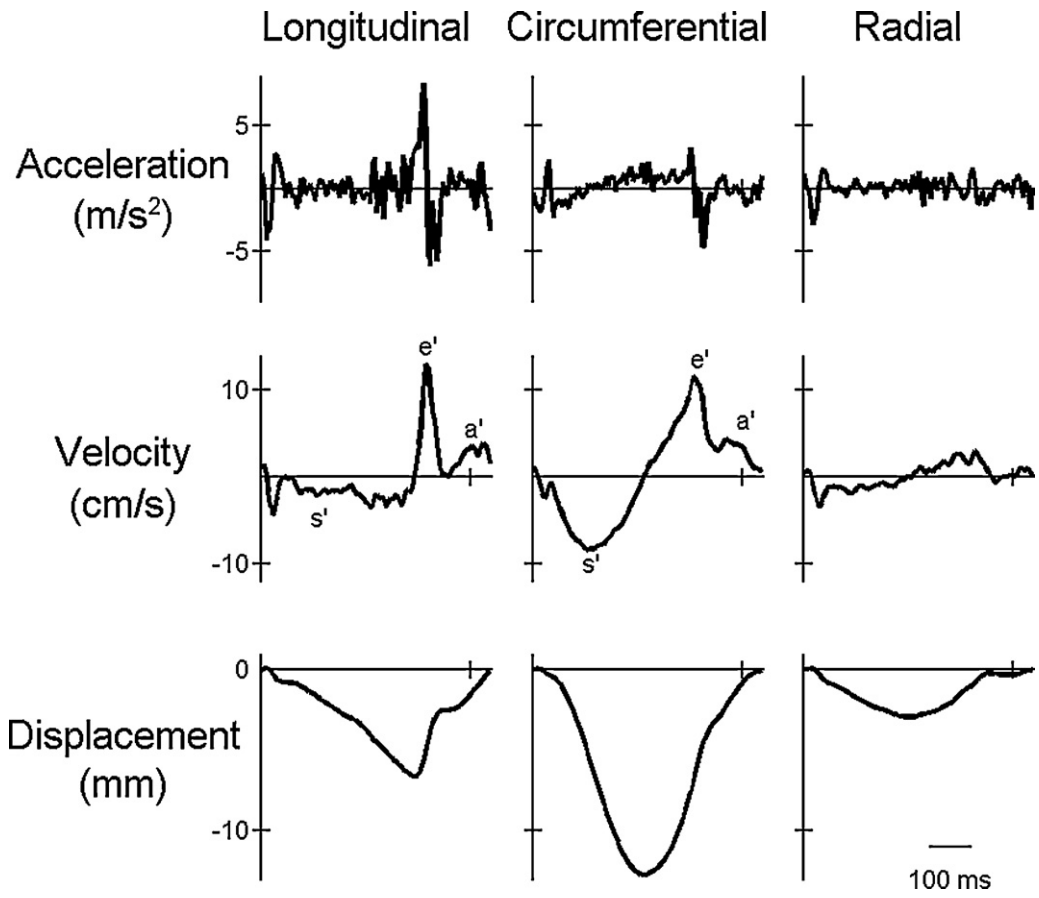

Fig. 4. Representative traces from the simulation model. Simulated measurements are extracted from a crystal placed in the anterior, apical region. The accelerometer axes are aligned as shown in Fig. 1. Mean acceleration over the cardiac cycle is subtracted, removing the average gravity component in the different directions. The systolic wave (s′), early (e′) and atrial induced filling waves (a′) are shown in the longitudinal and circumferential velocity traces.

Please cite this article in press as: Remme EW, et al. Simulation model of cardiac three dimensional accelerometer measurements. Med Eng Phys (2012), http://dx.doi.org/10.1016/j.medengphy.2012.04.015

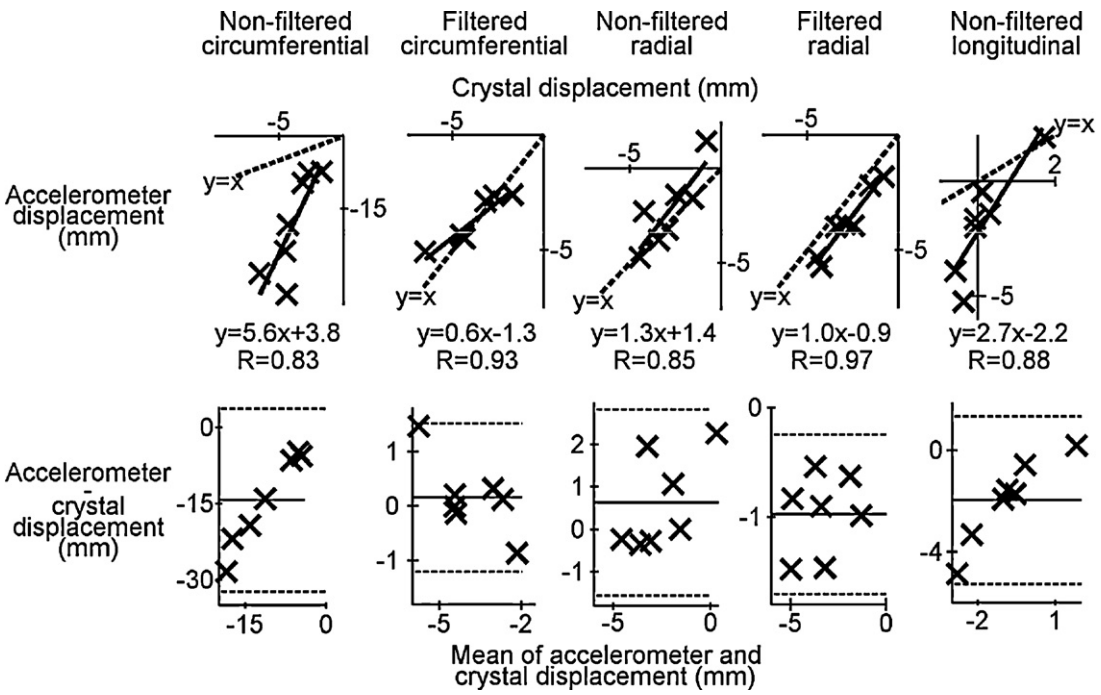

Fig. 5. Correlation (upper panel) and Bland-Altman (lower panel) plots of peak systolic displacement along the different accelerometer axes. The calculated displacement from the simulated accelerometer signal is compared to the true motion of a crystal attached at the same point as the accelerometer. The simulated measurements in the circumferential and radial directions are calculated without (non-filtered) and with (filtered) the algorithm for removing the time-varying gravity component. The mean error is indicated with the horizontal solid line in the Bland–Altman plot, while the dashed lines indicate mean error ± 1.96SD.

If compensation for the time-varying gravitation was not included, the simulation model overestimated circumferential velocity and displacement by about 4–5 times in the 7 animals (Fig. 5 left panel and Fig. 6), which was consistent with the overestimation observed in measurements from pigs [6]. Our proposed filtering algorithm to remove the gravity artifact predicted circumferential displacement with high accuracy. Peak systolic displacement correlated well ($R = 0.93$, $p < 0.01$) and differed marginally (0.2 ± 0.7 mm) from the true displacement (Fig. 5 second column panel). Fig. 6 shows true, non-filtered and filtered circumferential velocity and displacement traces from the simulation model. In our previous studies we have focused on circumferential motion which is the largest in the apical region where the accelerometer is attached. However, in this study we also investigated the accuracy of the radial and longitudinal axes (Fig. 5). In most cases true displacement and accelerometer derived displacement were in qualitative agreement along these 2 axes, however, there were 3 cases when the accelerometer derived displacement was in the opposite direction of the true displacement due to the gravity artifact. The filtering algorithm corrected this in the radial direction.

Table 1 shows the error of calculated peak systolic displacement using the simulated accelerometer signal with respect to the displacement of the crystal which mimicked the attached accelerometer at that point, first during standard accelerometer placement and orientation, and then during different situations. The estimated circumferential displacement using the gravity filtering method showed minor error with the true displacement in most cases. The estimation error was highest in the standing and sitting situations. The displacement was overestimated several times without the filtering, except in the standing position when circumferential motion occurred in the horizontal plane, i.e. with no gravity component. The error in the non-filtered estimate was relatively small also when the patient was lying on the left side. These results were consistent with our previous validation study of the accelerometer [6]. Circumferential displacement was

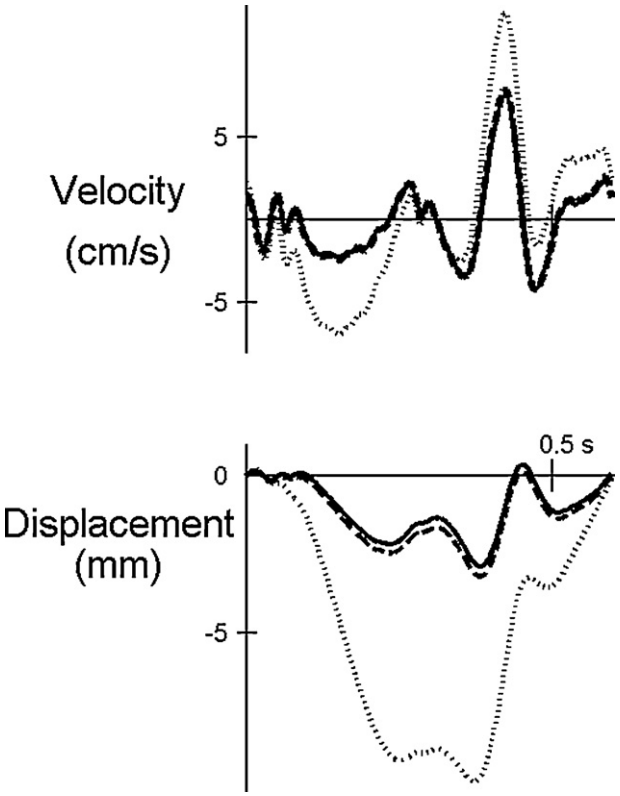

Fig. 6. Circumferential velocity and displacement traces from the simulation model. The dashed traces are the true motion of the accelerometer; solid lines are derived motion using the filtering algorithm to remove the time-varying gravity component; dotted lines are without the filtering algorithm. The dashed and solid lines are almost superimposed.

Please cite this article in press as: Remme EW, et al. Simulation model of cardiac three dimensional accelerometer measurements. Med Eng Phys (2012), http://dx.doi.org/10.1016/j.medengphy.2012.04.015

Table 1
Mean error ± SD (mm) and regression coefficient of calculated peak displacement using the simulated accelerometer signal versus the true motion of the crystal attached at the same point as the accelerometer during different situations ($n = 7$).

	Circumferential True displacement = −3.9 ± 1.5 mm		Radial True displacement = −2.9 ± 1.3 mm		Longitudinal True displacement = 0.1 ± 0.8 mm	
	Filtered	Non-filtered	Filtered	Non-filtered	Non-filtered	
Standard supine	0.2 ± 0.7	−14.4 ± 9.2	−1.0 ± 0.4	0.6 ± 1.1	−2.0 ± 1.7	
	$R = 0.93$	$R = 0.83$	$R = 0.97$	$R = 0.85$	$R = 0.88$	
Sitting	−1.0 ± 0.9	−10.2 ± 6.5	−2.4 ± 1.1	−0.8 ± 0.7	−1.0 ± 0.9	
	$R = 0.83$	$R = 0.85$	$R = 0.75$	$R = 0.90$	$R = 0.90$	
Standing	2.1 ± 1.2	0 ± 0	−1.9 ± 0.7	−1.7 ± 0.7	0.5 ± 0.4	
	$R = 0.64$	$R = 1.00$	$R = 0.89$	$R = 0.86$	$R = 0.86$	
Lying left side	0.6 ± 0.7	−1.4 ± 1.2	−1.2 ± 4.9	−13.6 ± 8.9	4.8 ± 2.7	
	$R = 0.90$	$R = 0.95$	$R = -0.63$	$R = -0.08$	$R = -0.38$	
+15° misalignment	0.4 ± 0.7	−13.3 ± 8.5	−2.0 ± 0.9	0.6 ± 1.1	−6.4 ± 4.0	
	$R = 0.93$	$R = 0.83$	$R = 0.85$	$R = 0.85$	$R = 0.66$	
−15° misalignment	0.2 ± 0.7	−14.3 ± 9.2	0.4 ± 0.6	0.6 ± 1.1	2.3 ± 2.7	
	$R = 0.92$	$R = 0.83$	$R = 0.94$	$R = 0.85$	$R = 0.09$	

the dominant motion and also most robustly estimated by the accelerometer. Radial displacement was generally also captured well by the accelerometer, but there were a couple of cases when the accelerometer indicated an outward displacement in contrast to the true inward displacement. The filtered radial displacement generally overestimated the inward motion by about 1–2 mm, but had slightly better correlation with the true displacement than the non-filtered. Longitudinal displacement was minor and the performance of the accelerometer was worst in this direction.

Mid-systolic circumferential velocity was reduced from 10.2 ± 4.9 cm/s at baseline to 5.6 ± 5.2 cm/s during ischemia while displacement was reduced from 10.6 ± 8.6 mm to 1.7 ± 10.2 mm (both $p < 0.05$). These results were consistent with our previous study in pigs [13] where the velocity was reduced from 13.2 ± 2.8 cm/s to 3.5 ± 1.8 cm/s and displacement from 11.5 ± 2.3 mm to −1.2 ± 2.8 mm.

4. Discussion

In the design and development of technological systems theoretical testing and mathematical simulation models may provide useful information and reduce the need and number of costly real life experiments. In this study we have developed a mathematical model that simulates the signal from a cardiac accelerometer. The model was based on previously measured cardiac motion and generated realistic 3 dimensional acceleration signals corresponding to the output of an accelerometer attached to the outer surface of the heart. The velocity and displacement that were calculated by integration of the simulated acceleration signal corresponded well with previous measurements from accelerometers attached to pig and human hearts. This suggests that the model, where the ground truth motion is known, may be applied to test new proposed methods to filter and process the accelerometer signal for extraction of clinical information.

The inclusion of the accelerometer axes rotation through the cardiac cycle is a key feature of the model for realistic simulation of the effect of gravity. The accelerometer signals coming from translation and from rotation in the gravitational field both have base frequency equal to the heart frequency, but the translational component has more of its energy in the higher harmonics of the heart rate. Integration with time is equivalent to division by frequency in the frequency domain, hence, amplifies lower and suppresses higher frequencies. When the accelerometer measurements are integrated, once to velocity and twice to position, the relative importance of the contribution from gravity increases relative to the contribution from translation. The model showed that double integration of acceleration to displacement substantially overestimated displacement relative to true displacement in the circumferential direction due to the time-varying gravity component.

The power spectrum of the simulated acceleration signals was for the most part similar to the spectrum of the measured signals from accelerometers implanted in actual hearts. There was a slight tendency to higher power at the high frequencies in the circumferential direction (Fig. 3, middle panel). This could potentially lead to low amplitude, high frequency noise in the simulated acceleration signal. However, when integrated to velocity and displacement, such high frequency noise is reduced. As the clinical information lies in the major wave features at low frequencies, small noise oscillations at high frequencies in the velocity and displacement traces have no clinical impact or interest. The calculated velocity and displacement from the simulated acceleration signal demonstrated similar features to the measurements obtained in our previous validation study of the accelerometer [6] including the same overestimation of peak systolic circumferential velocity

and displacement. The error caused by the time-varying gravity component was in the same range in the simulation model as we observed in the animal experiments which suggests that the prolate spheroidal method serves as a good approximation for simulation of accelerometer rotation. By applying our proposed gravity filtering algorithm the displacement was calculated with good accuracy compared to the true displacement in the model. Additionally in the previous validation study, different orientations of the accelerometer and positions of the patients were tested in a robot-experiment where the accelerometer was attached to a robot programmed to move like a point on the heart. The theoretical results of the current simulation model study were similar to the findings in the robot-study. Finally, the comparison between simulated measurements during baseline and ischemia showed a similar reduction of early systolic circumferential velocity and displacement as we have previously observed in pigs and humans [13]. The agreement between the simulation model and the findings in the previous studies with real accelerometer measurements suggests that the model provides realistically simulated measurements from an accelerometer placed on the heart wall.

Our simulation model for the accelerometer is novel in the sense that it is specific for cardiac motion and based on realistic motion from sonomicrometric crystal data. However, theoretical analysis of accelerometers for motion monitoring has been performed previously. Elble [14] performed a mathematical study on the impact of gravity on acceleration measurements of tremor and showed substantial gravitational artifact during rotational motion. His findings were similar to ours, but in contrast to the more random tremor motion, the relatively deterministic cyclic motion of the heart may be utilized in filters designed to correct for the gravity component. There have also been studies showing theoretically how combination of 2 or more 3-axes accelerometers may be used to quantify motion by separating the inertial and gravitational components of acceleration [15,16].

4.1. Limitations

The simulation model has only been validated in a qualitative manner which showed that the simulated velocity and displacement traces look realistic and that the error due to the gravity artifact is within the same range as shown in former studies. We have not been able to quantitatively validate the accuracy of the simulation model in a direct comparison study. We used sonomicrometric data from previous studies as input to the model. The motion in space of these crystals was not directly measured as the ultrasound crystals only measured distances relative to one another. However, the crystal software provided a mathematical conversion of these distances into 3D positions. A specified point that remained stationary, which the crystals moved relative to, was required for this conversion. We specified that the center of equator was stationary. If this point actually moved it will have introduced a time-varying offset between the simulated and true motion of the crystals. In a normal subject with intact pericardium and closed chest, the apex is often assumed to remain stationary. However, during open chest cardiac surgery with split pericardium the valve plane and apex typically contract towards the equator [17] which suggests that the equator is the more stationary region. Ideally, the crystal recordings should have been performed with inclusion of one or more crystals that were fixed in space. Thus, we would not have needed to make assumption where the stationary origin was as these fixed crystals could have been used. Such a crystal setup is difficult to implement as the fixed crystals cannot be placed far away due to limited signal strength, they must have direct "view" to the moving crystals (air or bones will block the signal), and proper fixation of these crystals is difficult. Thus, we have not been able to perform such a quantitative comparison study. However, the simulation model predicted the same findings as the findings from previous studies with the actual accelerometer. This indicates that the simulation model is realistic and may be applied it in our future work during initial testing of new algorithms to process the accelerometer signal.

The simulation model is based on measured motion of sonomicrometric crystals sutured to the epicardial wall, which is a highly invasive procedure only performed in animals. The accessibility to this type of measurements is low and thus limits the number of simulation cases based on this type of measurements. However, to estimate the motion of a point on the heart wall it may be possible to apply non-invasive measurements of rotation and longitudinal and radial displacement by e.g. echocardiography as an alternative approach. These 3 motions could be used as input for the θ, μ, λ-coordinates, respectively, and prescribe the changes in these coordinates during the cardiac cycle. A change in these coordinates is the same as motion in the prolate spheroidal space and would then serve as an estimate of the 3 dimensional motion of a point on the heart. The respective x, y, z-coordinates could be used in point #1 in the simulation procedure outlined as described in Section 2.3. The rest of the simulation procedure would be identical. This alternative procedure could potentially serve as a non-invasive based simulation model of the cardiac accelerometer and the echocardiographic recordings could be obtained from patients in a number of different situations.

Accelerometers will always have a small bias, e.g. at zero acceleration, the output will be slightly different from zero. If one desires to study the effects of bias or drifting, the simulated acceleration signal in Eq. (1) can be extended with an extra term on the right hand side that incorporates this feature. However, in our system this is a limited problem as the signal is high-pass filtered at a frequency just below the heart-rate frequency, which removes any bias or slow varying drift.

5. Conclusions

Based on previously measured motion of the heart we have developed a simulation model of an accelerometer attached to the surface of the heart. The model generated a simulated accelerometer signal which included both the translational motion of the accelerometer and also the time-varying gravity component which was due to rotation of the accelerometer axes as the accelerometer moves with the surface during the cardiac cycle. The simulated velocity and displacement from the model were consistent with actual measurements from previous studies during different situations including baseline and ischemia. This suggests that the simulation model may serve as a means to theoretically test new algorithms to filter and process the accelerometer measurements in our future work to extract clinical information from the sensor. The theoretical testing is expected to increase the efficiency of our work and reduce the need for animal experiments.

Funding

Anders Opdahl was recipient of a clinical research fellowship from the Norwegian Council on Cardiovascular Diseases, Oslo, Norway.

Acknowledgments

We would like to thank Dr Thomas Helle-Valle who kindly supplied us with the sonomicrometry data that were used in this study.

Appendix A. Supplementary data

Supplementary data associated with this article can be found, in the online version, at http://dx.doi.org/10.1016/j.medengphy.2012.04.015.

Conflict of interests

The three-axis accelerometer is patented by Oslo University Hospital, Rikshospitalet, Oslo, Norway, for the use of monitoring of myocardial function during and after cardiac surgery [18]. Engineer Ole Jakob Elle and Drs Erik Fosse and Per Steinar Halvorsen are patent holders. The company Cardiaccs AS has the rights to commercially exploit this idea. The other authors report no competing interests.

References

[1] Elle OJ, Halvorsen S, Gulbrandsen MG, Aurdal L, Bakken A, Samset E, et al. Early recognition of regional cardiac ischemia using a 3-axis accelerometer sensor. Physiol Meas 2005;26:429–40.
[2] Halvorsen PS, Espinoza A, Fleischer LA, Elle OJ, Hoff L, Lundblad R, et al. Feasibility of a three-axis epicardial accelerometer in detecting myocardial ischemia in cardiac surgical patients. J Thorac Cardiovasc Surg 2008;136:1496–502.
[3] Halvorsen PS, Fleischer LA, Espinoza A, Elle OJ, Hoff L, Skulstad H, et al. Detection of myocardial ischaemia by epicardial accelerometers in the pig. Br J Anaesth 2009;102:29–37.
[4] Comunale ME, Body SC, Ley C, Koch C, Roach G, Mathew JP, et al. The concordance of intraoperative left ventricular wall-motion abnormalities and electrocardiographic S–T segment changes: association with outcome after coronary revascularization. Multicenter Study of Perioperative Ischemia (McSPI) Research Group. Anesthesiology 1998;88:945–54.
[5] Slogoff S, Keats AS. Does chronic treatment with calcium entry blocking drugs reduce perioperative myocardial ischemia? Anesthesiology 1988;68:676–80.
[6] Remme EW, Hoff L, Halvorsen PS, Nærum E, Skulstad H, Fleischer LA, et al. Validation of cardiac accelerometer sensor measurements. Physiol Meas 2009;30:1429–44.
[7] Imenes K, Aasmundtveit K, Husa EM, Høgetveit JO, Halvorsen S, Elle OJ, et al. Assembly and packaging of a three-axis micro accelerometer used for detection of heart infarction. Biomed Microdevices 2007;9:951–7.
[8] Hoff L, Elle OJ, Grimnes M, Halvorsen S, Alker HJ, Fosse E. Measurements of heart motion using accelerometers. Conf Proc IEEE Eng Med Biol Soc 2004:2049–51.
[9] Helle-Valle T, Remme EW, Lyseggen E, Pettersen E, Vartdal T, Opdahl A, et al. Clinical assessment of left ventricular rotation and strain: a novel approach for quantification of function in infarcted myocardium and its border zones. Am J Physiol Heart Circ Physiol 2009;297:H257–67.
[10] Opdahl A, Helle-Valle T, Remme EW, Vartdal T, Pettersen E, Lunde K, et al. Apical rotation by speckle tracking echocardiography: a simplified bedside index of left ventricular twist. J Am Soc Echocardiogr 2008;21:1121–8.
[11] Helle-Valle T, Crosby J, Edvardsen T, Lyseggen E, Amundsen BH, Smith HJ, et al. New noninvasive method for assessment of left ventricular rotation: speckle tracking echocardiography. Circulation 2005;112:3149–56.
[12] Nielsen PM, Le Grice IJ, Smaill BH, Hunter PJ. Mathematical model of geometry and fibrous structure of the heart. Am J Physiol Heart Circ Physiol 1991;260:H1365–78.
[13] Halvorsen PS, Remme EW, Espinoza A, Skulstad H, Lundblad R, Bergsland J, et al. Automatic real time detection of myocardial ischemia by epicardial accelerometer. J Thorac Cardiovasc Surg 2010;139:1026–32.
[14] Elble RJ. Gravitational artifact in accelerometric measurements of tremor. Clin Neurophysiol 2005;116:1638–43.
[15] Padgaonkar AJ, Krieger KW, King AI. Measurement of angular acceleration of a rigid body using linear accelerometers. J Appl Mech 1975;42:552–6.
[16] Hayes WC, Gran JD, Nagurka ML, Feldman JM, Oatis C. Leg motion analysis during gait by multiaxial accelerometry: theoretical foundations and preliminary validations. J Biomech Eng 1983;105:283–9.
[17] Skulstad H, Andersen K, Edvardsen T, Rein KA, Tønnessen TI, Hol PK, et al. Detection of ischemia and new insight into left ventricular physiology by strain Doppler and tissue velocity imaging: assessment during coronary bypass operation of the beating heart. J Am Soc Echocardiogr 2004;17:1225–33.
[18] Elle OJ, Fosse E, Gulbrandsen MG. International patent application with international publication number WO 03/061473 2003.

Please cite this article in press as: Remme EW, et al. Simulation model of cardiac three dimensional accelerometer measurements. Med Eng Phys (2012), http://dx.doi.org/10.1016/j.medengphy.2012.04.015